Measurement 147 (2019) 106822

Contents lists available at ScienceDirect

Measurement

journal homepage: www.elsevier.com/locate/measurement

Telecentricity based measurement error compensation in the bilateral telecentric system

Wenjie Li, Jianmei Wu, Dong Li, Yong Tian, Jindong Tian *

Key Laboratory of Optoelectronic Devices and Systems of Education Ministry and Guangdong Province, College of Optoelectronic Engineering, Shenzhen University, 518060 Shenzhen, China

ARTICLE INFO

Article history:
Received 8 April 2019
Received in revised form 3 June 2019
Accepted 14 July 2019
Available online 16 July 2019

Keywords:
Geometry measurement
Telecentricity
Bilateral telecentric system
Machine vision

ABSTRACT

A stable magnification, low distortions, and a wide depth of field (DoF) make a bilateral telecentric system well-suited for geometrical measurements with a large scope of working distances. However, a limitation of such a telecentric system appear because the magnification changes slightly for different working distances even within the DoF, which results in the measurement error. Therefore, we propose a method to compensate the measurement error in telecentricity. The parameters of the measurement error caused by the telecentricity are analyzed in detail and experiments are implemented to verify the flexibility of the proposed method. Our results show that the stability of the magnification at different working distances is improved after the compensation of the telecentricity error. We believe that our approach can significantly improve the precision of geometrical measurements through the error compensation caused by telecentricity.

1. Introduction

Machine vision technology can measure or detect objectives geometry size automatically and intelligently through the advantages of a non-contact, high precision, and fast process while avoiding human error, which makes it popular in many industrial fields [1–6]. Ali et al. [7] developed a machine vision software to improve the measurement of the precision in machining. Peng et al. used detection algorithms for computer vision technology to control the quality of O-rings [8]. Xiang et al. [9] presented a measurement method using a two-camera machine vision system and a relative measurement principle to achieve a high-accuracy assessment of the sizes of bayonets in large automobile brake pads.

Machine vision technology includes an optical imaging system, a mechanical element, a control system, and image processing. Among them, the optical imaging system obtains the information from the measured object directly and contributes the most to the precision of the measurement. Usually, a high image resolution is required when measuring or inspecting an object. However, the depth of field (DoF) gets narrower as the resolution increases. A narrow DoF might be incompatible for tasks where different working distances are needed such as for geometry measurements in different planes. Moving the camera or the measured object can solve the problem but the images acquired need to be processed separately. Extending the DoF becomes imperative, especially for microscope imaging. Shain et al. extended the DoF of a microscope imaging system using a deformable mirror [10,11].Using the liquid crystal lens to modulate the image system, Chen et al. also can get an extended DoF [12]. Fitzgerald et al. [13] doubled the DoF of a low-cost iris recognition front-facing camera in mobile phones by introducing intrinsic primary chromatic aberrations in the lens and using a dual-wavelength illumination. All these methods are generally not used for macroscopic measurements because of the low extended DoF and the changing magnification in the frame.

Although a non-telecentric lens has a large field of view, it suffers from high distortions, a narrow DoF, and perspective errors. In contrast, a telecentric lens offers a high resolution, nearly zero distortion, a wide DoF, and a stable magnification. For high precision requirements, telecentric optical systems are becoming increasingly popular in machine vision [14–18]. Schuster et al. [19] compared the influence of the distortion and the perspective errors in a traditional and a telecentric optical system and concluded that the telecentric lens had a better measurement precision. Zhang et al. [20] obtained a fine measurement of a complex surface profile using a bilateral telecentric lens. The measurement precision was sub-pixel after optimizing the algorithm. Pan et al. [21] obtained a similar result by comparing the images of traditional lens and a bilateral telecentric lens. Although the image plane was out of place because of the temperature, the bilateral telecentric lens

* Corresponding author.
E-mail address: jindt@szu.edu.cn (J. Tian).

https://doi.org/10.1016/j.measurement.2019.07.050
0263-2241/

formed an image with sub-pixel resolved. Overall, the telecentric lens system performs very well to measure object sizes, especially when different working planes are involved. Theoretically, the chief rays are parallel to the optical axis in the bilateral telecentric system and the magnification is constant within the DoF. When a bilateral telecentric system is used, the magnification is calibrated accurate only in one location in the DoF and later used in the whole DoF. However, because of the manufacturing and assembly errors in the telecentric lens, the chief rays and the optical axis have, in reality, a small angle, which is called telecentricity. The magnification of a bilateral telecentric system is affected by the telecentricity and changes slightly even within the DoF, resulting in a measurement error for different working distances [22]. A typical value of telecentricity is 0.1°, which will cause a radial measurement error of about 1.7 μm when the measured object moves 1 mm along optical axis in the DoF. If the DoF is 10 mm, the maximum measurement error may be up to 17 μm in the DoF, which cannot meet some requirements for high precision measurements. Such a radial measurement error is related to axial position so that the magnification changes for different working distances. Methods to improve the measurement precision, such as calibration and image processing, are only suitable for one working plane and insensitive to a change in the working distance. Once the geometry to be measured deviates from the corrected plane, a measurement error is caused by the telecentricity.

Fortunately, the magnification does not vary in the same working plane and it is possible to establish a relationship between the magnification and the working distance based on the telecentricity. Thus, the magnification can be corrected and a higher precision measurement can be obtained. Consequently, we can propose a method for high-precision geometry measurement based on the telecentricity to improve the overall precision. First, we analyzed the telecentricity. Then, the theoretical parameters of the telecentricity compensation are determined. Finally, we verified the predictions experimentally.

2. Analysis of the telecentricity

A lens can be telecentric in the image space, object space, or both to reduce perspective errors. Fig. 1 shows a bilateral telecentric system. The focal point of the group of lenses 1 (image side) coincides with the focal point of the group of lenses 2 (object side). An aperture stop is added at the common focal point to ensure that the chief rays are parallel to the optical axis. The object to measure is imaged perpendicularly and the magnification theoretically constant. Usually, an accurate magnification is obtained by calibration with a camera at one position of the DoF. It is considered constant in the whole DoF. However, as shown in Fig. 2, the aperture stop does not always fully coincide with the ideal position after assembly of all the components of the bilateral telecentric lens, which leads to a small deviation between the chief rays and the optical axis. This small angular deviation α is the telecentricity. Due to the telecentricity α, the system magnification slightly changes when the working distance changes, which will affect the measurement. As shown in Fig. 2, the measured objects L_0, L_1, and L_2 with the same length at different working distances have different images with sizes L_0', L_1', and L_2' although all images obtained in the DoF are fine. Fortunately, the telecentricity is invariable once the bilateral telecentric system is assembled. It is possible to establish a relationship between the magnification and the working distance based on the telecentricity. Then, the telecentricity can be compensated to get a high precision geometry measurement at different working distances.

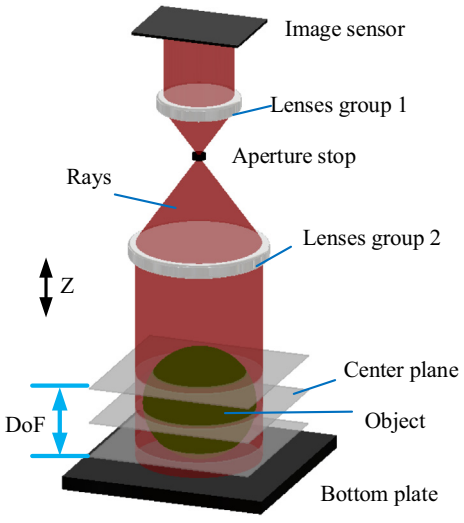

Fig. 1. Principle of a bilateral telecentric optical system.

In Fig. 2, the object L_0 is at the object focal plane of lens group 1 and the size of its image is not affected by the telecentricity. This focal plane is defined as the center plane, where the center of the DoF is located. The system magnification M_0 in the center plane is:

$$M_0 = \frac{f_2}{f_1} \tag{1}$$

where, f_1, and f_2 are the focal lengths of the two group lenses, respectively. We can easily get the value of M_0 through calibration with a camera. The accurate expression for an object with a nominal length L at the working distance l is:

$$L = \frac{L'}{M_0} + \alpha(l - l_0) \tag{2}$$

where, α is the telecentricity of bilateral telecentric system. L' is the image size in the working distances l. M_0 result from the calibration of the magnification at the working distance l_0. Eq. (2) corrects the system magnification according the working distance to keep the measurement invariable. It is necessary to calibrate the telecentricity to get a high precision measurement.

3. System analysis

3.1. Center plane

Before the telecentricity can be calibrated, camera calibration is performed to get M_0. The image is the sharpest in the center plane, which is suitable for camera calibration. We use the image sharpness evaluation function to find the center plane. There are many

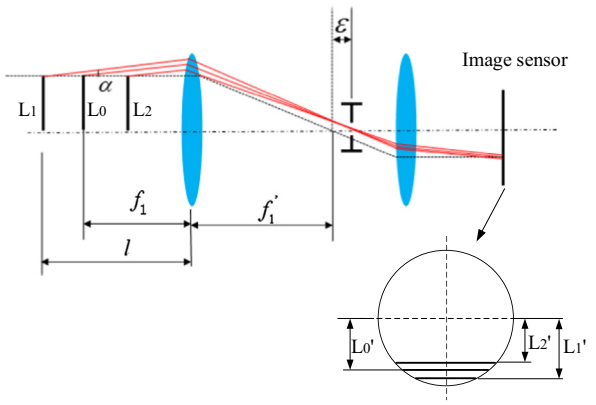

Fig. 2. Telecentricity of bilateral telecentric optical system.

methods for evaluating the image sharpness [23–29]. Among them, the gradient sharpness function has a low computing complexity and can be expressed by [28,29]:

$$S = \frac{1}{2mn}\sum_{x,y}\{[i(x,y) - i(x-1,y)]^2 + [i(x,y) - i(x,y-1)]^2\} \tag{3}$$

where S is the calculated sharpness value, i(x, y) is the intensity at pixel (x, y), and m and n are the numbers of rows and columns, respectively. The differences in the average intensity between pixel (x, y) and its neighbor pixels $(x-1, y)$ and $(x, y-1)$ are computed. The computed value for each pixel is added together to calculate S that is then divided by the number of pixels. For each acquired image, the image sharpness S of the selected pattern is computed and plotted as a function of the image serial number.

3.2. System calibration

There are many available studies on camera calibration in the image system [30–34]. The pinhole model of a wide angle cameras is not suitable for telecentric image systems because of the orthographic projection in the telecentric lenses. The projection of an arbitrary point P to a computer image coordinate is expressed as:

$$\begin{matrix} x_u \\ [y_u] \\ 1 \end{matrix} = \begin{matrix} \frac{m}{du} & 0 & 0 & r_1 & r_2 & t_x \\ 0 & \frac{m}{dv} & 0 & r_3 & r_4 & t_y \\ 0 & 0 & 1 & 0 & 0 & 1 \end{matrix} \begin{matrix} X_w \\ [Y_w] \\ Z_w \end{matrix} \tag{4}$$

When taking the radial and thin prism distortions into consideration, we have:

$$\begin{cases} \delta_x = k_1 x_u (x_u^2 + y_u^2) + s_1 (x_u^2 + y_u^2) \\ \delta_y = k_1 y_u (x_u^2 + y_u^2) + s_2 (x_u^2 + y_u^2) \\ \begin{bmatrix} (u - u_0)du \\ (v - v_0)dv \end{bmatrix} = \begin{bmatrix} x_u \\ y_u \end{bmatrix} + \begin{bmatrix} \delta_x \\ \delta_y \end{bmatrix} \end{cases} \tag{5}$$

where, (x_u, y_u) are the image coordinates, (u, v) are the pixel coordinates, and du, dv are the pixel sizes in the × and y direction, respectively. (u_0, v_0) denotes the pixel position of the origin point O that is usually the center of the image plane. m is the magnification of the telecentric lens. r_i (i = 1–4) are the elements of the rotation matrix R and t_x t_y are the elements of the translation matrix. (X_w, Y_w, Z_w) is the object point P coordinate in the world coordinate system. High precision calibration procedures have been presented in our previously published work [30,35] that took the radial and thin prism distortions into consideration in detail.

During telecentricity calibration, an object with a nominal length L is measured in the entire DoF. According to Eq. (2):

$$L' = \mathrm{M_0L} - \alpha \mathrm{M_0}(l - l_0) \tag{6}$$

The image size varies linearly with the working distance l. A series of images with sizes L' at different working distances l is obtained using a precision translation device in the DoF. Then, a linear fit is performed and the telecentricity is the slope of the fitting line.

3.3. Depth of field (DoF)

As shown in Fig. 3, we also analyzed the DoF of the system to determine the range of the working distance [36]. If d is the diameter of a fuzzy dot in the object space, the index f denotes a point far away, and the index n denotes a near point, we obtain through geometric considerations:

$$\frac{\Phi_{\mathrm{EP}}}{d_f} = \frac{p_f}{(p_f - p)} \tag{7}$$

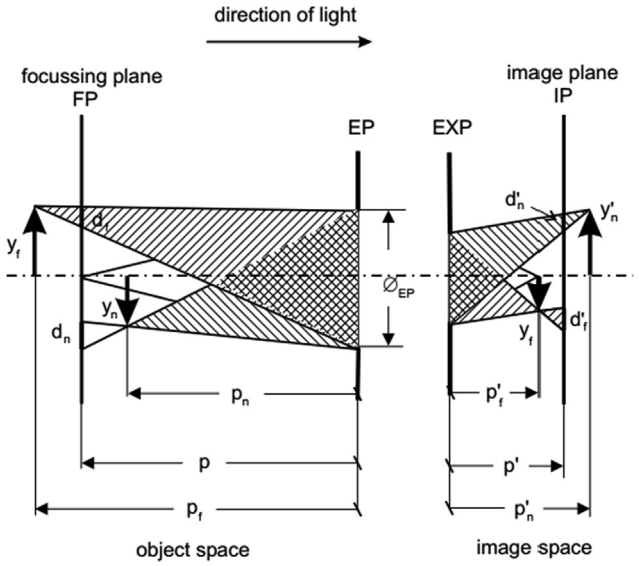

Fig. 3. Analysis of DoF.

$$\frac{\Phi_{\mathrm{EP}}}{d_n} = \frac{p_n}{(p - p_n)} \tag{8}$$

From Gaussian optics, we have:

$$\beta_p = \frac{\varnothing_{EXP}}{\varnothing_{EP}} \tag{9}$$

$$\frac{\beta_p}{p'} - \frac{1}{\beta_p \cdot p} = \frac{1}{f'} \tag{10}$$

$$F = \frac{f'}{\varnothing_{EP}} \tag{11}$$

$$d' = \beta \mathrm{d_f} = \beta \mathrm{d_n} \tag{12}$$

where β_p is the pupil magnification ratio, Φ_{EP} and Φ_{EXP} are the diameters of the entrance pupil and the exit pupil, respectively, and F, f', and d' are the f number, the image focus, and the diameter of the permission fuzzy dot, respectively. From Eq. (10), we obtain:

$$p = f'\left(\frac{1}{\beta} - \frac{1}{\beta_{\mathrm{p}}}\right) \tag{13}$$

According the formulas (7)–(13), we obtain the DoF as a function of the magnification:

$$DoF = \frac{2(1 - \frac{\beta}{\beta_p})Fd'}{\beta^2 - \frac{F^2 d'^2}{f'^2}} \tag{14}$$

For bilateral telecentric systems, the entrance pupil EP and the exit pupil EXP have to be at infinity. The DoF of the bilateral telecentric systems is:

$$DoF = \frac{2(1 - \frac{\beta}{\beta_p})}{\beta^2 - \frac{F^{\#2} d'^2}{f'^2}} = \lim_{x \to \infty} \frac{2(\frac{1-\beta}{\beta_p})\frac{f'}{\varnothing_{EP}}}{\beta^2 - \frac{d'^2}{\varnothing_{EP}^2}} = \frac{2f'(\frac{1}{\beta} - \frac{1}{\beta_p})\frac{d'}{\varnothing_{EP}}}{\beta} = \frac{2d'}{\beta}\frac{p}{\varnothing_{EP}} = \frac{d'}{\beta \sin\theta} \tag{15}$$

where θ is the aperture. Unfortunately, d' and θ are not the parameters directly measured. In air, A = sinθ where A is the numerical aperture. The relationship between the numerical aperture and the effective f number F is:

$$F = \frac{\beta}{2A} \tag{16}$$

According to Eqs. (15) and (16), we have:

$$DoF = \frac{2d'\mathrm{F}}{\beta^2} \tag{17}$$

In Eq (17), the diameter of the permission fuzzy dot d' is an empirical parameter that is related to the pixel size in practical applications. An estimation of *DoF* for a telecentric optical system can be expressed as [37]:

$$DoF = \frac{pkF}{\beta^2} \tag{18}$$

where p, k, and F are the pixel size, the experience parameter, and the effective f number, respectively. For size measurements, $k = 0.008$ whereas $k = 0.015$ for defect inspection.

The working distance l is also an important parameter for the compensation of the measurement error caused by the telecentricity according to Eq. (2). In many cases, this parameter is known in the measurement. The precision requirement for the determination of the working distance is not very high according to Eq. (2). The working distance can also be obtained using common measurement tools like a Vernier caliper. There are also many precision methods to measure Δl, including binocular vision and phase measurement technology [35,38,39]. In this work, the working distance is obtained with high accuracy from the precision translation device used to verify the validity of the proposed method.

In this section, we analyzed theoretically the parameters of the measurement error compensation for the telecentricity. The calibration method for the camera and the telecentricity for the center plane are exposed in detail. To get a fine compensation in the DoF or the extended DoF, we performed an analysis of the DoF in the bilateral telecentric system. A validation experiment was carried out to verify the validity and the flexibility of our theoretical formulation.

4. Experiment

To verify the validity of the proposed method, a measurement experiment using the telecentricity compensation was carried out, as shown in Fig. 4. The measurement system consisted of a calibration plate, a piezoelectric (PZT) translation device, and the bilateral telecentric system. The camera and the bilateral telecentric lens were from Basler and Opto Engineering, respectively. Their main parameters are shown in Table 1. According to Eq. (18), the DoF of the designed telecentric system was about 4 mm when used in the size measurement mode. A ceramics plate with a highly precise circle pattern was chosen for calibration. The central distance of the adjacent circle pattern was 3 mm. A PZT translation device was used to provide the precision movement of the calibration plate along the z direction, thereby simulating a geometry measurement at different working distances. The range and the precision of the PZT translation device were 0–13 mm and 0.05 μm, respectively.

Given the parameters of the lens, the distance between the lens and the calibration plate was adjusted when the PZT device was in its middle position (z = 6.5 mm), which allows moving the calibration plate in both directions from the center plane. For a typical value of the telecentricity of 0.1 degree, the measurement error of 0.2 mm per step is less than 0.3 μm according to Eq. (2), which is acceptable. We imaged the calibration plate in the z range of 0–13 mm with a step size of 0.2 mm to acquire 66 pictures.

Fig. 5 shows the images sharpness after normalization. The 33rd image is the center plane according to the comparison of the image sharpness. There, the position of the PZT device is z = 6.4 mm. We then set the center plane as the origin plane, defined now as z = 0 mm to perform the camera calibration in this plane according to our method [30] to obtain the internal and external parameters of the camera. The calibration result is given in Table 2.

After the camera calibration, the calibration of the telecentricity is performed in the DoF, as presented in Fig. 6. A length L_0 including ten dots is chosen as the calibration object (Fig. 6 (a)). The red stars

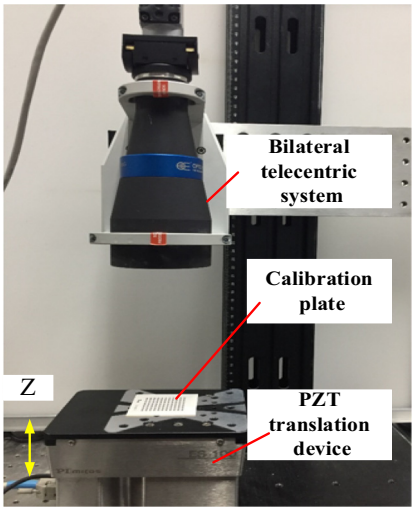

Fig. 4. Measurement device setup used.

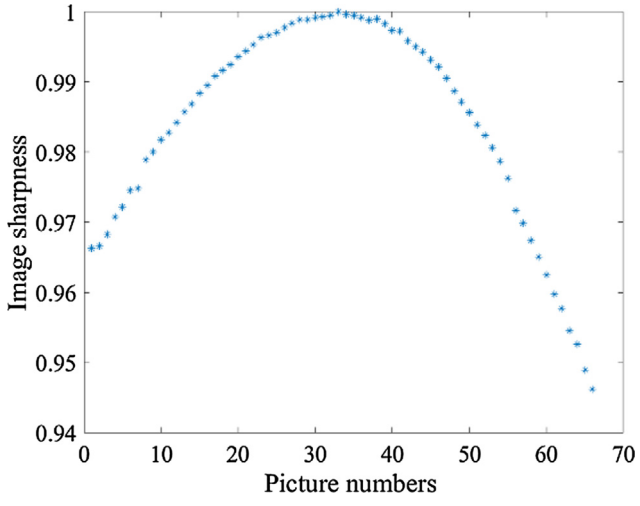

Fig. 5. Analysis of the picture sharpness values for different working distances simulated by the position of the PZT.

Table 1
Main parameters of the camera and the telecentric lens.

	Type	Pixel size	Pixels	Magnification	*F* number
Camera	acA2500-14gm GigE	2.2 μm	5 million	–	–
Telecentric lens	TCSM048	–	–	0.184	8

Table 2
Camera calibration parameters.

Magnification M_0	Origin point $[u_0,v_0]$	Distortion $[k_1, k_2, s_1,s_2]$	Rotation R = $[r_i]$	Translation T = $[t_x, t_y]$
0.1848	[1313.2, 887.3]	$10^{-5} \times$ [1.61, −0.047, 0.72, −2.84]	[−1.00000 , 0.00047–0.00047, −1.00000]	[0.025, 1.04]

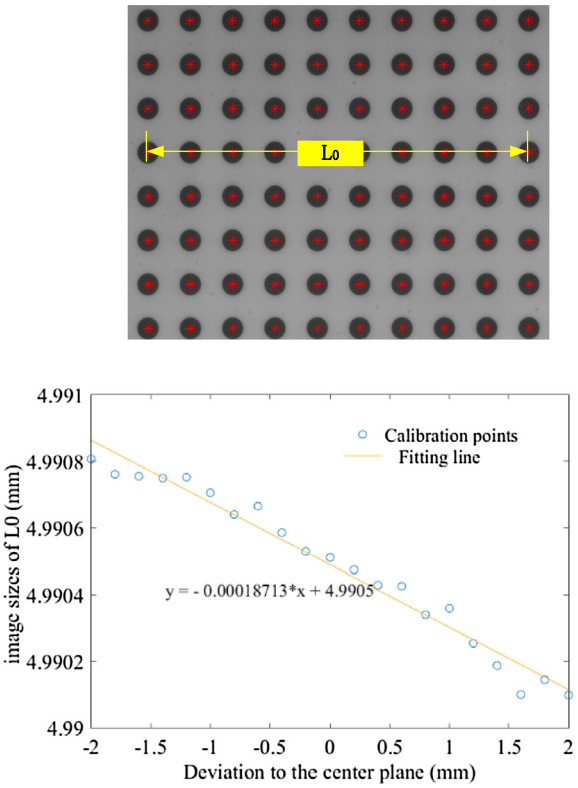

Fig. 6. (a) Calibration object used for the telecentricity with the characteristic length L_0 = 27 mm. (b) Linear fit to determine the telecentricity.

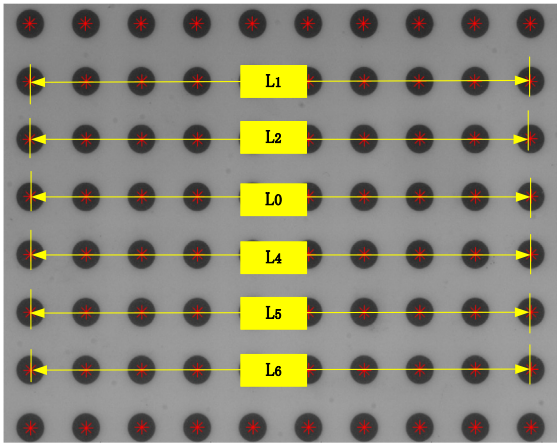

Fig. 7. Measured objects.

represent the centers of every circle determined by a high precision algorithm. Nominally, L_0 = 27 mm.

The telecentricity calibration result is presented in Fig. 6 (b). The value of the horizontal ordinate is the deviation between the working plane and the calibration plane, which is defined as $\Delta l = (l - l_0)$. The size of the image of L_0 decreased linearly when the working distance increased, which verifies the theoretical prediction made. The slope of the fitting line is −0.0001871 and the lens telecentricity is −0.001 rad according to Eq (6). Consequently, Eq. (2) can now be expressed as:

$$L = \frac{L'}{0.1848} - 0.001 \times \Delta l \tag{19}$$

Six lines with lengths of L_1, L_2, L_0, L_4, L_5, and L_6 on the calibration plate were chosen as the data to measure in the DoF and twice the DoF to verify the accuracy of the telecentricity calibration, as shown in Fig. 7. The nominal values obtained were all 27 mm. The average value defined the measured length. When the calibration plate moves along the optical axis thanks to the translation device, the object geometry was measured at different working distances.

Fig. 8(a) shows the measurements before and after telecentricity compensation for 21 measured values of different working planes in the DoF. The RANGE (maximum-minimum error) parameter was chosen to characterize the fluctuations of the measurement results. It decreased significantly from about 3.8 μm to about 0.45 μm. The stability of the magnification was effectively improved. The detailed data is given in Table 3. The maximum and the minimum are, respectively, the differences where the maximum and minimum values deviate from the nominal value. We use the root mean square error (RMSE) of 21 measurement values in the DoF to describe the measurement precision. The precision was improved three times. This showed that error compensation with the telecentricity can keep the system magnification stable and significantly improve the precision of the geometry measurement in the DoF.

Fig. 8(b) shows the results of the measurement for 41 measured values of different working planes in twice the DoF. After telecentricity compensation, the RANGE of the measurements obtained was reduced by 5.9 μm, from 7.6 μm to 1.7 μm. The RMSE was improved 4 times, from 2.2 μm to 0.5 μm. The detailed comparison is presented in Table 4. The precision in twice the DoF is almost the same as in the DoF. The telecentricity error compensation can extend the DoF and still provide high precision.

We also used a standard block to verify the flexibility of the proposed method. The width and height of the standard block were both 10 mm. It had a fine precision in the direction of the width, as presented in Fig. 9(a). The standard block also moves along the optical axis to simulate an object at different working distances. As shown in Fig. 9(b), the RANGE of the measurement increases up to 16.2 μm in twice the DoF when the telecentricity measurement error is not compensated. With telecentricity compensation, the RANGE is reduced by 7.3 μm, which represents about 1 μm improvement in the radial measurement precision when the difference in working distances is 1 mm. The detailed data is presented in Table 5 where Z is the distance between the center plane and the object plane. Δ_{BC} and Δ_{AC} are the differences between the measured and nominal widths of the standard block (10 mm) before and after telecentricity compensation, respectively. After telecentricity compensation, the RMSE improved from 4.3 μm to 2.2 μm and was roughly doubled. Our data implies that error compensation using the telecentricity is necessary to achieve a precise measurement.

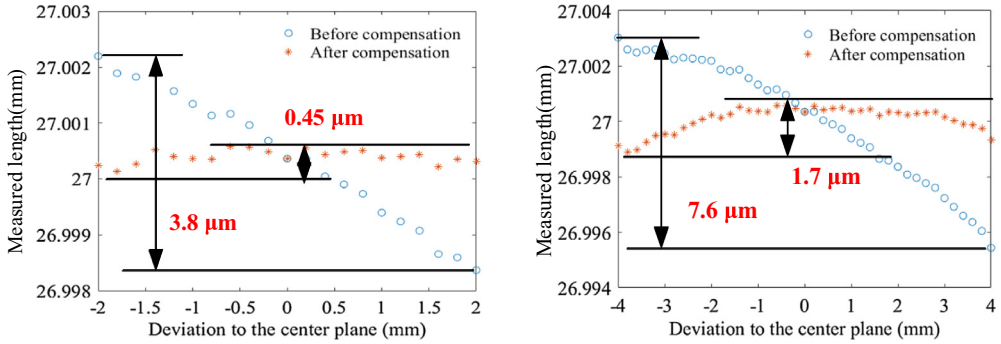

Fig. 8. Analysis of the measurement error (a) in the DoF and (b) twice the DoF.

Table 3
Measurement error in the DoF. Unit: μm.

	Maximum	Minimum	RANGE	RMSE
Before compensation	2.2	−1.6	3.8	1.2
After compensation	0.58	0.13	0.45	0.4

Table 4
Measurement error in twice the DoF. Unit: μm.

	Maximum	Minimum	RANGE	RMSE
Before compensation	3.0	−4.6	7.6	2.2
After compensation	0.7	−1.0	1.7	0.5

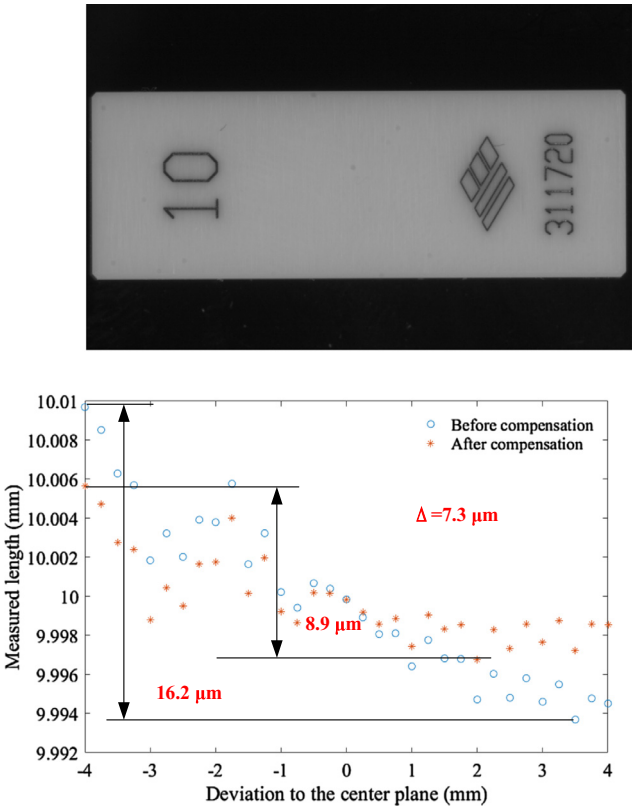

Fig. 9. (a) Photograph of the standard block used and (b) results from the error compensation.

Table 5
Results of the measurement of the standard block in twice the DoF.

Z (mm)	−4	−3	−2	−1	0	1	2	3	4	RANGE	RMSE
Δ_{BC} (μm)	9.7	1.9	3.8	1.2	−0.1	−3.6	−5.3	−5.4	−5.5	16.2	4.3
Δ_{AC} (μm)	5.7	−1.2	1.8	−0.8	−0.1	−2.6	−3.2	−2.4	1.4	8.9	2.2

5. Conclusion

In this study, we analyzed the influence of the telecentricity on the geometry measurement in a bilateral telecentric system. A method for error compensation based on the telecentricity was proposed to maintain a stable magnification in the DoF and twice the DoF. The comparison of the measurements before and after the telecentricity error compensation validated our method. The proposed method significantly improves the measurement precision in the DoF and extends the DoF, which is attractive for the use of bilateral telecentric systems in machine vision.

The telecentricity based error compensation in the bilateral telecentric system is suit for size measurement for the tasks with some thickness or with different heights in the industrial field. It is also one of our further research directions.

Declaration of Competing Interest

None.

Acknowledgments

The authors would like to appreciate the financial support from the National Natural Science Foundation of China (61727814, 51775352).

References

[1] Mark Quinn, Emanuele Spinosa, David Roberts, Miniaturisation of pressure-sensitive paint measurement systems using low-cost, miniaturised machine vision cameras, Sensors 17 (8) (2017) 1708.
[2] X.W. Ye, C.Z. Dong, T. Liu, A review of machine vision-based structural health monitoring: methodologies and applications, J. Sens. 2016 (2016) 1–10.
[3] Xinyu Li, Tiezhu Qiao, Yusong Pang, et al., A new machine vision real-time detection system for liquid impurities based on dynamic morphological characteristic analysis and machine learning, Measurement 124 (2018) 130–137.
[4] Xu Yan, James M.W. Brownjohn, Review of machine-vision based methodologies for displacement measurement in civil structures, J. Civ. Struct. Health Monit. 8 (1) (2018) 91–110.
[5] Wu. Xiaojun, Guangming Gao, LED light design method for high contrast and uniform illumination imaging in machine vision, Appl. Opt. 57 (7) (2018) 1694.
[6] Jun Yang, Xuekun Li, Xu. Jirui, et al., Development of an optical defect inspection algorithm based on an active contour model for large steel roller surfaces, Appl. Opt. 57 (10) (2018) 2490.
[7] Md. Hazrat Ali, Syuhei Kurokawa, Kensuke Uesugi, Camera based precision measurement in improving measurement accuracy, Measurement 49 (2014) 138–147.

[8] Gaoliang Peng, Zhujun Zhang, Weiquan Li, Computer vision algorithm for measurement and inspection of O-rings, Measurement 94 (2016) 828–836.
[9] Rong Xiang, Wenhui He, Xinna Zhang, et al., Size measurement based on a two-camera machine vision system for the bayonets of automobile brake pads, Measurement 122 (2018) 106–116.
[10] William J. Shain, Nicholas A. Vickers, Jiang Li, et al., Axial localization with modulated-illumination extended-depth-of-field microscopy, Biomed. Opt. Exp. 9 (4) (2018) 1771.
[11] W.J. Shain, N.A. Vickers, B.B. Goldberg, et al., Extended depth-of-field microscopy with a high-speed deformable mirror, Opt. Lett. 42 (5) (2017) 995–998.
[12] Hung-Shan Chen, Yi-Hsin Lin, An endoscopic system adopting a liquid crystal lens with an electrically tunable depth-of-field, Opt. Exp. 21 (15) (2013) 18079.
[13] Niamh M. Fitzgerald, Christopher Dainty, Alexander V. Goncharov, Extending the depth of field with chromatic aberration for dual-wavelength iris imaging, Opt. Exp. 25 (25) (2017) 31696.
[14] A. Miks, J. Novak, Design of a double-sided telecentric zoom lens, Appl. Opt. 51 (24) (2012) 5928–5935.
[15] Yang Tong, Jin Guofan, Zhu Junguo, Design of image-side telecentric freeform imaging systems based on a point-by-point construction-iteration process, Chin. Opt. Lett. 15 (6) (2017) 77–81.
[16] Junzheng Peng, Meng Wang, Dingnan Deng, et al., Distortion correction for microscopic fringe projection system with Scheimpflug telecentric lens, Appl. Opt. 54 (34) (2015).
[17] Wu. Lifu, Jianguo Zhu, Huimin Xie, Single-lens 3D digital image correlation system based on a bilateral telecentric lens and a bi-prism: validation and application, Appl. Opt. 54 (26) (2015) 7842.
[18] Xia Liu, Zhenyu Liu, Guifang Duan, et al., Precise and robust binocular camera calibration based on multiple constraints, Appl. Opt. 57 (18) (2018) 5130.
[19] Thomas Schönheit, Norbert Schuster, Influence of the machine vision lens to the accuracy in contactless 2D-metrology, Proc. SPIE 4902 (2002) 294–305.
[20] Wu Yang, Xiaofeng Zhou, Yichi Zhang, in: High Precision Size Measurement System of Industrial Profiles Section, IEEE, 2015, pp. 415–419.
[21] Bing Pan, Yu. Liping, Wu. Dafang, High-accuracy 2D digital image correlation measurements with bilateral telecentric lenses: error analysis and experimental verification, Experim. Mech. 53 (9) (2013) 1719–1733.
[22] Bartosz Powałka, Tomasz Chady, Michał Szydłowski, Object's Optical Geometry Measurements Based on Extended Depth of Field (EDoF) Approach, AIP, 2017, 110026.
[23] Yunli Li, Wu. Junjie, Pu. Wei, et al., An autofocus method based on maximum image sharpness for Fast, in: Factorized Back-projection, IEEE, 2017, pp. 1201–1204.
[24] Yan Tian, Yili Yin, Li Zhang, An improved image sharpness assessment method based on contrast sensitivity, SPIE (2015), 967531-967535.
[25] Yuhua Li, Liqiang Ren, Yuchen Qiu, Objective evaluation of the microscopic image sharpness for diagnostic metaphase chromosomes, SPIE (2013), 85820I-85821I.
[26] Fang Qian, Jin Guo, Tao Sun, et al., Quantitative assessment of laser-dazzling effects through wavelet-weighted multi-scale SSIM measurements, Opt. Laser Technol. 67 (2015) 183–191.
[27] Hong-ning Li, Xu. Lin-li, Jie Feng, et al., Sharpness evaluation function of wavelength-related multi-spectral image, IEEE (2013) 452–456.
[28] S. Bres, J.M.E. Loupias, Digital image processing, Computing (1998) 265–275.
[29] R. Redondo, G. Bueno, G. Cristobal, et al., Quality evaluation of microscopy and scanned histological images for diagnostic purposes, Micron 43 (2–3) (2012) 334–343.
[30] Dong Li, Jindong Tian, An accurate calibration method for a camera with telecentric lenses, Opt. Lasers Eng. 51 (5) (2013) 538–541.
[31] Beiwen Li, Song Zhang, Flexible calibration method for microscopic structured light system using telecentric lens, Opt. Exp. 23 (20) (2015) 25795.
[32] Li Rao, Feipeng Da, Weiqi Kong, et al., Flexible calibration method for telecentric fringe projection profilometry systems, Opt. Exp. 24 (2) (2016) 1222.
[33] Haibo Liu, Huijing Lin, Linshen Yao, Calibration method for projector-camera-based telecentric fringe projection profilometry system, Opt. Exp. 25 (25) (2017) 31492.
[34] Shourui Yang, Miao Liu, Jiahui Song, et al., Flexible digital projector calibration method based on per-pixel distortion measurement and correction, Opt. Lasers Eng. 92 (2017) 29–38.
[35] Dong Li, Chunyang Liu, Jindong Tian, Telecentric 3D profilometry based on phase-shifting fringe projection, Opt. Exp. 22 (26) (2014) 31826.
[36] K. Lenhardt, Handbook of Machine Vision, 2006.
[37] https://www.opto-engineering.com/resources/faqs#q15 [Z].
[38] Min Zhong, Feng Chen, Chao Xiao, et al., 3D surface profilometry based on 2D S-Transform method with optimized window, Optik – Int. J. Light Electron Opt. 139 (2017) 87–94.
[39] Zhenqi Niu, Nan Gao, Zonghua Zhang, et al., 3D shape measurement of discontinuous specular objects based on advanced PMD with bi-telecentric lens, Opt. Exp. 26 (2) (2018) 1615.